Available online at www.sciencedirect.com
SCIENCE DIRECT®
Journal of Computational Physics 203 (2005) 386–404
JOURNAL OF COMPUTATIONAL PHYSICS
www.elsevier.com/locate/jcp

Vertical discretizations for compressible Euler equation atmospheric models giving optimal representation of normal modes

J. Thuburn *, T.J. Woollings

Department of Meteorology, University of Reading, P.O. box 243 , Earley Gate, Reading, RG6 6BB, UK

Received 11 June 2004; received in revised form 27 August 2004; accepted 28 August 2004
Available online 23 September 2004

Abstract

Accurate representation of different kinds of wave motion is essential for numerical models of the atmosphere, but is sensitive to details of the discretization. In this paper, numerical dispersion relations are computed for different vertical discretizations of the compressible Euler equations and compared with the analytical dispersion relation. A height coordinate, an isentropic coordinate, and a terrain-following mass-based coordinate are considered, and, for each of these, different choices of prognostic variables and grid staggerings are considered. The discretizations are categorized according to whether their dispersion relations are optimal, are near optimal, have a single zero-frequency computational mode, or are problematic in other ways. Some general understanding of the factors that affect the numerical dispersion properties is obtained: heuristic arguments concerning the normal mode structures, and the amount of averaging and coarse differencing in the finite difference scheme, are shown to be useful guides to which configurations will be optimal; the number of degrees of freedom in the discretization is shown to be an accurate guide to the existence of computational modes; there is only minor sensitivity to whether the equations for thermodynamic variables are discretized in advective form or flux form; and an accurate representation of acoustic modes is found to be a prerequisite for accurate representation of inertia-gravity modes, which, in turn, is found to be a prerequisite for accurate representation of Rossby modes.

Keywords: Staggered grids; Vertical coordinates; Atmospheric waves

* Corresponding author.
E-mail addresses: j.thuburn@rdg.ac.uk (J. Thuburn), t.j.woollings@rdg.ac.uk (T.J. Woollings).

0021-9991/$ - see front matter © 2004 Elsevier Inc. All rights reserved.
doi:10.1016/j.jcp.2004.08.018

1. Introduction

In the design of numerical models for simulating atmospheric flow there is considerable freedom in the choice of vertical coordinate. For models solving the compressible Euler equations, height-based coordinates and their terrain-following variants (e.g. [3,6,9,23,25,28–30]) and terrain-following mass-based coordinates ([4,17,19,37]) have been proposed. For models solving the hydrostatic primitive equations, as well as height and mass or pressure-based coordinates, an entropy-based or "isentropic" coordinate (e.g. [16]), and a Lagrangian coordinate [21] have been proposed, and it appears to be possible to extend these to the compressible Euler equations. Particular vertical coordinates have the potential to reduce numerical errors by simplifying or eliminating one or more terms in the governing equations, e.g. vertical advection terms are eliminated in a Lagrangian vertical coordinate, or by facilitating discrete analogues of conservation properties. There is ongoing debate over which vertical coordinate is best. For any given vertical coordinate there is considerable freedom in the choice of predicted variables. For example, temperature T or potential temperature θ may be chosen as one of the thermodynamic variables. Again there is ongoing debate over which choice of variables is best (e.g. [25]). There is also some freedom in how the predicted variables are arranged in space when the equations are discretized; possibilities include the A- to E-grids [1] and Z-grid [24,35] in the horizontal and the Lorenz [22] and Charney–Phillips [5] grids in the vertical. Once again there is ongoing debate over which choice is best (e.g. [12,13,33]). These three issues are inextricably linked; the optimal grid staggering will depend on the choice of vertical coordinate and predicted variables, and so on. We must therefore seek the optimal overall configuration of vertical coordinate, predicted variables, *and* grid.

Many criteria are relevant when deciding on the optimal configuration. These criteria include conservation properties and coupling between the equations for the resolved dynamics and the parameterized physics. In this paper, we concentrate on the ability of different candidate configurations to simulate accurately the normal modes of the linearized, adiabatic and frictionless governing equations, particularly their dispersion properties. Large-scale atmospheric flow is close to hydrostatic balance (or its generalization known as quasi-hydrostatic balance) and to geostrophic balance (or its non-linear generalization). When any forcing mechanism tends to perturb the flow away from balance it responds by radiating acoustic and inertia-gravity waves, which disperse and dissipate, thus tending to restore balance: a process known as "adjustment". In numerical models, accurate representation of the vertical structure of acoustic modes is essential for correct simulation of adjustment to, and maintenance of (quasi-) hydrostatic balance. Accurate representation of the vertical structure of inertia-gravity modes is essential for correct simulation of adjustment to, and maintenance of, geostrophic balance or its non-linear generalization. Accurate representation of acoustic and inertia-gravity mode frequencies is usually considered less crucial; for example, reduction of mode frequencies due to the use of semi-implicit time stepping, e.g. [15], is usually considered to be relatively harmless. However, it will slow the adjustment process, and is also expected to exaggerate the spontaneous emission of inertia-gravity waves by artificially increasing the frequency matching between the balanced and unbalanced components of the flow [11,26]. Accurate representation of both the structure and frequency of Rossby modes is essential because they are meteorologically significant in their own right. One widely discussed type of dispersion error occurs for discretizations that support a "computational mode": for an idealized background state a non-zero pattern of disturbance, typically comprising a vertical two-grid-length oscillation in the thermodynamic variables, can be invisible to the discretization and therefore does not propagate [33]; consequently, the scheme cannot support a steady response to a steady forcing that projects onto that mode [27]; in more complex situations the computational modes can be unphysically unstable [2]. Computational modes can be suppressed by numerical filtering, but the filtering itself can be damaging, for example disrupting conservation properties. Another important type of dispersion error occurs when the numerical dispersion relation is so distorted that some part of the wave spectrum has group velocity of the wrong sign, implying propagation of energy in the wrong direction (e.g. [10]).

In this paper, we concentrate on the choice of thermodynamic variables, and on the choice of vertical coordinate and grid staggering. It is assumed, for now, that this problem can be considered separately from the complementary problem of the choice of wind variables and horizontal grid staggering. We address the full compressible Euler equations, since approximate equation sets such as anelastic or hydrostatic are known to be accurate only over a limited range of horizontal scales [8].

In height coordinates there are two heuristic arguments suggesting that the optimal configuration for normal modes will use potential temperature θ and pressure p as thermodynamic prognostic variables, with u, v and p staggered relative to w and θ. (We introduce the shorthand notation $(w\theta, uvp)$ for this configuration, with the obvious generalization to other configurations.) The first argument is based on the analytical vertical structure of the normal modes [7,31]. For each mode, the vertical structures of u, v and p have the same zeros, and the vertical structures of w and θ have the same zeros. Moreover, the zeros of u, v and p alternate with those of w and θ and, in the limit of large vertical wavenumber, fall exactly half way between them. The $(w\theta, uvp)$ configuration would therefore be the most economical way of representing such vertical structures, as noted in [31].

The second argument is based on consideration of the difference equations for the candidate configurations. Inaccuracies may be introduced whenever a variable is averaged from unstaggered levels to staggered levels or vice-versa, and whenever vertical derivatives are approximated by differences over an interval $2\Delta z$ rather than Δz. The $(w\theta, uvp)$ configuration minimizes such inaccuracies: all vertical derivatives are approximated by differences over Δz, and only part of the buoyancy term in the w equation (and the vertical advection of p for the advective form of the p equation—see Sections 2.2, 2.5, and 6) involve vertical averages.

These two arguments are only heuristic. A definitive answer requires the normal modes to be computed and compared for the different candidate configurations. Such a comparison is one of the aims of this paper. For small-amplitude perturbations about an isothermal state of rest the normal modes and their dispersion relation can be found analytically. We therefore compute numerically the normal modes for each candidate configuration and compare them with the analytical normal modes. Configurations with good dispersion properties and no computational modes are identified. A further aim is to extend the analysis to other vertical coordinates, namely a Lagrangian coordinate and a terrain-following mass-based coordinate. The optimal and near-optimal configurations for the different vertical coordinates are compared.

2. Governing equations

2.1. General vertical coordinate

The Euler equations for a deep spherical atmosphere, written in terms of a general vertical coordinate s, are given by [36]. Here, we simplify by approximating the geometry as a tangent plane at latitude ϕ. We make the shallow-atmosphere approximation, so that the $2\Omega\cos\phi$ Coriolis terms associated with the horizontal component of the Earth's rotation vector are neglected (where Ω is the Earth's rotation rate). Also, to begin with, we neglect β, the northward gradient of the Coriolis parameter $f = 2\Omega\sin\phi$; we will include it later. Moist effects and diabatic heating and friction are also neglected, and the equations are linearized about a reference state (indicated by superscript (r)) at rest and in hydrostatic balance. The governing equations are then as follows:

$$u_t - fv + \frac{p_x}{\rho^{(r)}} + gz_x = 0, \tag{1}$$

$$v_t + fu + \frac{p_y}{\rho^{(r)}} + gz_y = 0, \tag{2}$$

$$w_t + \frac{1}{\sigma^{(r)}}(g\sigma + p_s) = 0, \tag{3}$$

$$z_t + \dot{s} z_s^{(r)} - w = 0, \tag{4}$$

$$\theta_t + \dot{s}\theta_s^{(r)} = 0, \tag{5}$$

$$\sigma_t + \sigma^{(r)}(u_x + v_y) + \left(\dot{s}\sigma^{(r)}\right)_s = 0, \tag{6}$$

$$\rho_t + \dot{s}\rho_s^{(r)} + \rho^{(r)}\nabla\cdot\mathbf{u} = 0, \tag{7}$$

$$T_t + \dot{s}T_s^{(r)} + \frac{\kappa T^{(r)}}{1-\kappa}\nabla\cdot\mathbf{u} = 0, \tag{8}$$

$$p_t + \dot{s}p_s^{(r)} + \frac{p^{(r)}}{1-\kappa}\nabla\cdot\mathbf{u} = 0. \tag{9}$$

Here, u, v and w are the velocity components, $\dot{s} = Ds/Dt$ is the rate of change of s following a fluid parcel, $z^{(r)}$, $\theta^{(r)}$, $\rho^{(r)}$, $T^{(r)}$ and $p^{(r)}$ are the reference profiles of height, potential temperature, density, temperature and pressure (all functions of s only), $\sigma^{(r)} = \rho^{(r)}\mathrm{d}z^{(r)}/\mathrm{d}s$ is the reference profile of the mass per unit "volume" in x–y–s space, and z, θ, ρ, T, p and σ are the perturbations to these quantities. Subscripts x, y, s and t indicate partial derivatives, and $\nabla.\mathbf{u} = u_x + v_y + w_s/z_s^{(r)}$. The constant $\kappa = R/C_p$ where R is the gas constant for dry air and C_p is the specific heat capacity at constant pressure.

We seek solutions in a domain with rigid boundaries at height 0 and height D. The appropriate boundary conditions are that w must vanish at the top and bottom boundaries. We will consider only coordinate systems in which the top and bottom boundaries are coordinate surfaces; then $\dot{s}$ must vanish at the top and bottom boundaries. It then follows that z_t and θ_t must also vanish at the top and bottom boundaries.

The six quantities z, θ, ρ, T, p and σ play the role of thermodynamic variables. They are not all independent, since they are related by the linearized definition of σ

$$\frac{\sigma}{\sigma^{(r)}} = \frac{\rho}{\rho^{(r)}} + \frac{z_s}{z_s^{(r)}}, \tag{10}$$

the linearized ideal gas law

$$\frac{p}{p^{(r)}} = \frac{T}{T^{(r)}} + \frac{\rho}{\rho^{(r)}}, \tag{11}$$

the linearized definition of potential temperature

$$\frac{\theta}{\theta^{(r)}} = \frac{T}{T^{(r)}} - \kappa\frac{p}{p^{(r)}}, \tag{12}$$

and the definition of the vertical coordinate. Thus, there are only two degrees of freedom in the thermodynamic variables, and so only two of equations (4)–(9) should be used; if needed, the thermodynamic variables that are not predicted must be diagnosed from (10)–(12) and the coordinate definition.

Not all combinations of predicted thermodynamic variables are possible, and the allowed combinations depend on the choice of vertical coordinate. For example, in a height coordinate z itself obviously cannot be predicted, while in an isentropic coordinate T and ρ are not independent of p so only one of these three can be predicted.

The six possible thermodynamic variables considered here certainly do not exhaust the possibilities. (Indeed one further possibility, the Montgomery potential $M = gz + C_pT$ is considered in Section 2.3.)

However, many of the plausible alternative choices are equivalent, or virtually equivalent, under the linear normal mode analysis to the cases being considered. For example, using specific entropy is equivalent to using potential temperature, since the specific entropy perturbation is proportional to the potential temperature perturbation; and using density times temperature, density times potential temperature, or Exner function are each equivalent to using pressure. Note, also, that for linearization about a state of rest, using wind components is equivalent to using momentum components, since the perturbation to the eastward momentum is $\rho^{(\mathrm{r})}u$, etc. Further, since we will consider only vertical discretizations, using horizontal wind components is equivalent to using the vertical component of vorticity and the horizontal divergence.

We now specialize to three particular vertical coordinates: a height coordinate, a Lagrangian coordinate (which reduces to an isentropic coordinate for the simple basic state considered), and a terrain-following mass-based coordinate. Note that the same physical system, with the same physical boundary conditions, is being modeled in each case; in particular, the true frequencies of the normal modes will be independent of the coordinate system used.

2.2. Height coordinate

In a height coordinate the height perturbation z is identically zero, σ becomes identical to ρ, and $\dot{s} = w$. The governing equations then become:

$$u_{\mathrm{t}} - fv + \frac{1}{\rho^{(\mathrm{r})}} p_x = 0, \tag{13}$$

$$v_{\mathrm{t}} + fu + \frac{1}{\rho^{(\mathrm{r})}} p_y = 0, \tag{14}$$

$$w_{\mathrm{t}} + \frac{1}{\rho^{(\mathrm{r})}} (g\rho + p_z) = 0, \tag{15}$$

$$\theta_{\mathrm{t}} + w\theta_z^{(\mathrm{r})} = 0, \tag{16}$$

$$\rho_{\mathrm{t}} + w\rho_z^{(\mathrm{r})} + \rho^{(\mathrm{r})} \nabla \cdot \mathbf{u} = 0, \tag{17}$$

$$T_{\mathrm{t}} + wT_z^{(\mathrm{r})} + \frac{\kappa T^{(\mathrm{r})}}{1-\kappa} \nabla \cdot \mathbf{u} = 0, \tag{18}$$

$$p_{\mathrm{t}} + wp_z^{(\mathrm{r})} + \frac{p^{(\mathrm{r})}}{1-\kappa} \nabla \cdot \mathbf{u} = 0. \tag{19}$$

We may choose any two of the four thermodynamic variables θ, ρ, T, and p to be our predicted variables, giving six possible pair choices to consider.

2.3. Isentropic coordinate

In a Lagrangian vertical coordinate $\dot{s} \equiv 0$ so that the prognostic equation for σ simplifies and all vertical advection terms vanish. For the horizontally uniform basic state studied here a Lagrangian coordinate is an isentropic coordinate. In this case the potential temperature perturbation is identically zero, and p, ρ and T are not independent so, of these three, we will consider only p as a predicted variable. Using T or ρ instead would be equivalent to using p in the analysis. In addition, we consider

the Montgomery potential $M = gz + C_p T$ as a possible thermodynamic variable; in an isentropic coordinate the geopotential plus pressure gradient term has a natural and concise expression in terms of M, so there might be some advantage to be gained by using it. The governing equations then become:

$$u_t - fv = -\left(\frac{p_x}{\rho^{(r)}} + g z_x\right) = -M_x, \tag{20}$$

$$v_t + fu = -\left(\frac{p_y}{\rho^{(r)}} + g z_y\right) = -M_y, \tag{21}$$

$$w_t = -\frac{1}{\sigma^{(r)}}(g\sigma + p_\theta) = -\frac{1}{z_\theta^{(r)}}\left(M_\theta - \frac{\kappa \Pi^{(r)}}{p^{(r)}} p\right), \tag{22}$$

$$z_t - w = 0, \tag{23}$$

$$\sigma_t + \sigma^{(r)}(u_x + v_y) = 0, \tag{24}$$

$$p_t + \frac{p^{(r)}}{1-\kappa}\nabla \cdot \mathbf{u} = 0, \tag{25}$$

$$M_t + \frac{RT^{(r)}}{1-\kappa}\nabla \cdot \mathbf{u} - gw = 0, \tag{26}$$

where $\Pi^{(r)} = C_p(p^{(r)}/p_0)^\kappa$ is the reference profile of the Exner function and $p_0 = 10^5$ Pa is the constant reference pressure used in the definition of potential temperature. We may choose any two of the four thermodynamic variables z, σ, p, and M to be our predicted variables, giving six possible pair choices to consider. Note, however, that the choice of σ and M together requires the solution of a set of non-local simultaneous equations for p and z. These must be solved by forming an equation for z

$$\frac{z_\theta}{z_\theta^{(r)}} - \frac{g(1-\kappa)}{RT^{(r)}} z = \frac{\sigma}{\sigma^{(r)}} - \frac{(1-\kappa)}{RT^{(r)}} M, \tag{27}$$

and integrating from either the bottom or top boundary where $z = 0$. For the full equations without linearization this problem would be non-linear as well; the σ–M combination might therefore be unattractive even if it had good dispersion properties.

Note that the pressure gradient and buoyancy terms can be expressed either in terms of p, z and σ (which we call the p-form) or in terms of M and p (which we call the M-form). When discretized, the two forms are not generally equivalent, so we consider both.

2.4. Terrain-following mass-based coordinate

The vertical coordinate $s = \eta$ is defined to be the mass of atmosphere per unit area above the given location divided by the mass of atmosphere per unit area in the entire atmospheric column [36]. Thus, the top and bottom boundaries are coordinate surfaces with $\eta = 0$ at the top boundary and $\eta = 1$ at the bottom boundary. This definition implies

$$\sigma^{(r)} = -\int_0^D \rho^{(r)}\,\mathrm{d}z \tag{28}$$

and

$$\sigma = -\int_0^D \rho \, \mathrm{d}z, \tag{29}$$

so both $\sigma^{(\mathrm{r})}$ and σ are independent of η.

The governing equations become:

$$u_\mathrm{t} - fv + \frac{p_x}{\rho^{(\mathrm{r})}} + g z_x = 0, \tag{30}$$

$$v_\mathrm{t} + fu + \frac{p_y}{\rho^{(\mathrm{r})}} + g z_y = 0, \tag{31}$$

$$w_\mathrm{t} + \frac{1}{\sigma^{(\mathrm{r})}}\left(g\sigma + p_\eta\right) = 0, \tag{32}$$

$$z_\mathrm{t} + \dot{\eta} z_\eta^{(\mathrm{r})} - w = 0, \tag{33}$$

$$\theta_\mathrm{t} + \dot{\eta}\theta_\eta^{(\mathrm{r})} = 0, \tag{34}$$

$$\rho_\mathrm{t} + \dot{\eta}\rho_\eta^{(\mathrm{r})} + \rho^{(\mathrm{r})}\nabla \cdot \mathbf{u} = 0, \tag{35}$$

$$T_\mathrm{t} + \dot{\eta} T_\eta^{(\mathrm{r})} + \frac{\kappa T^{(\mathrm{r})}}{1-\kappa}\nabla.\mathbf{u} = 0, \tag{36}$$

$$p_\mathrm{t} + \dot{\eta} p_\eta^{(\mathrm{r})} + \frac{p^{(\mathrm{r})}}{1-\kappa}\nabla \cdot \mathbf{u} = 0. \tag{37}$$

An expression for $\dot{\eta}$ is obtained by taking the vertical integral of the equation for σ_t

$$\sigma_\mathrm{t} + \sigma^{(\mathrm{r})}(u_x + v_y) + \left(\dot{\eta}\sigma^{(\mathrm{r})}\right)_\eta = 0, \tag{38}$$

and using the fact that σ is independent of η, giving

$$\sigma_\mathrm{t} = -\int_0^1 \sigma^{(\mathrm{r})}(u_x + v_y)\, \mathrm{d}\eta \tag{39}$$

and

$$\dot{\eta} + \eta\frac{\sigma_\mathrm{t}}{\sigma^{(\mathrm{r})}} + \int_0^\eta (u_x + v_y)\, \mathrm{d}\eta = 0. \tag{40}$$

However, not all configurations require the use of a separate prognostic equation (39) for σ_t. First note that z and ρ are not independent, because of (10) and the fact that σ is now independent of η. So z and ρ cannot both be predicted variables. If z is not a predicted variable then ρ is either a predicted variable or can be deduced from the other predicted thermodynamic variables. For consistency, the tendency of σ should then be deduced from the (explicit or implied) tendency of ρ using (29). If, on the other hand, z is a predicted variable, then ρ cannot be a predicted variable, nor can it be deduced from the predicted variables without knowledge of σ. Therefore, a separate equation (39) is needed to predict σ. We must choose two of the five thermodynamic variables z, θ, ρ, T, and p to be predicted variables, but z and ρ cannot be used together, so there are nine possible pair choices to consider.

2.5. Flux-form thermodynamic equations

By using (4) to eliminate $\dot{s}$ and rearranging to incorporate w entirely in the divergence terms, Eqs. (7)–(9) can be rewritten in flux-form (for ρ) or a form that looks similar to flux-form (for T and p):

$$\rho_t - z_t \frac{\rho_s^{(r)}}{z_s^{(r)}} + \nabla \cdot \left(\rho^{(r)}\mathbf{u}\right) = 0, \tag{41}$$

$$T_t - z_t \frac{T_s^{(r)}}{z_s^{(r)}} + \frac{\kappa T^{(r)(2-1/\kappa)}}{1-\kappa} \nabla \cdot \left(T^{(r)(1/\kappa-1)}\mathbf{u}\right) = 0, \tag{42}$$

$$p_t - z_t \frac{p_s^{(r)}}{z_s^{(r)}} + \frac{p^{(r)\kappa}}{1-\kappa} \nabla \cdot \left(p^{(r)(1-\kappa)}\mathbf{u}\right) = 0. \tag{43}$$

In some configurations this can reduce the amount of vertical averaging required, particularly in a height coordinate for which the z_t terms vanish. The effect of using the flux-forms rather than the advective forms (7)–(9) is discussed in Section 6.

2.6. Equations for wavelike modes

If f is constant then all coefficients in (1)–(12) are independent of x, y and t, so their solutions can be Fourier decomposed into horizontally wavelike oscillations proportional to $\exp \mathrm{i}(kx + ly - \omega t)$. Assuming a solution of this form, the height-coordinate equations (13)–(19) become:

$$-\mathrm{i}\omega u - fv + \frac{1}{\rho^{(r)}} \mathrm{i}kp = 0, \tag{44}$$

$$-\mathrm{i}\omega v + fu + \frac{1}{\rho^{(r)}} \mathrm{i}lp = 0, \tag{45}$$

$$-\mathrm{i}\omega w + \frac{1}{\rho^{(r)}} p_z + \frac{g\rho}{\rho^{(r)}} = 0, \tag{46}$$

$$-\mathrm{i}\omega\theta + w\theta_z^{(r)} = 0, \tag{47}$$

$$-\mathrm{i}\omega\rho + w\rho_z^{(r)} + \rho^{(r)}(\mathrm{i}ku + \mathrm{i}lv + w_z) = 0, \tag{48}$$

$$-\mathrm{i}\omega T + wT_z^{(r)} + \frac{\kappa T^{(r)}}{1-\kappa}(\mathrm{i}ku + \mathrm{i}lv + w_z) = 0, \tag{49}$$

$$-\mathrm{i}\omega p + wp_z^{(r)} + \frac{p^{(r)}}{1-\kappa}(\mathrm{i}ku + \mathrm{i}lv + w_z) = 0. \tag{50}$$

Analogous equations may be written for the θ-coordinate and terrain-following mass-based coordinate cases.

2.7. Inclusion of the β-effect

On an f-plane there is no β-effect and therefore no Rossby restoring mechanism, so all Rossby modes have zero frequency. Rossby modes are meteorologically important, so it is desirable to be able to assess

how well candidate configurations represent them. However, if we simply replace the constant f in (1) and (2) by a linear latitude variation $f = f_0 + \beta y$ then solutions proportional to $\exp \mathrm{i}(kx + ly - \omega t)$ are no longer possible.

We can include the β-effect while still retaining constant-coefficient equations by approximating f and β as constants in an appropriate way so as to maintain an energetically consistent equation set. Begin with (1) and (2) but regard f as a function of latitude. Take the horizontal divergence and vertical component of the curl of these equations to obtain

$$\xi_t + f\delta + \beta v = 0, \tag{51}$$

$$\delta_t - f\xi + \beta u + \nabla_H^2\left(\frac{p}{\rho^{(r)}} + gz\right) = 0, \tag{52}$$

where $\xi = v_x - u_y$, $\delta = u_x + v_y$, and ∇_H^2 is the "horizontal" Laplacian operator holding s fixed. From now on regard f and β as constants. In order to retain energy conservation βu must be replaced by βu_{div} and βv must be replaced by βv_{rot}, where subscripts "div" and "rot" refer to the divergent and rotational components of the wind field; see, e.g. [34] for a detailed discussion. Now solutions proportional to $\exp \mathrm{i}(kx + ly - \omega t)$ are possible. For such solutions (51) and (52) become

$$-\mathrm{i}\omega(\mathrm{i}kv - \mathrm{i}lu) + f(\mathrm{i}ku + \mathrm{i}lv) + \beta v_{rot} = 0, \tag{53}$$

$$-\mathrm{i}\omega(\mathrm{i}ku + \mathrm{i}lv) - f(\mathrm{i}kv - \mathrm{i}lu) + \beta u_{div} - K^2\left(\frac{p}{\rho^{(r)}} + gz\right) = 0, \tag{54}$$

where $K^2 = k^2 + l^2$. Then, undoing the divergence and curl to obtain equations for u and v tendencies, and using the fact that the divergent flow is irrotational and the rotational flow is non-divergent, so that $\mathrm{i}ku_{rot} + ilv_{rot} = 0$ and $\mathrm{i}kv_{div} - \mathrm{i}lu_{div} = 0$, gives

$$-\mathrm{i}\omega u - fv - \frac{ik\beta}{K^2}u + ik\left(\frac{p}{\rho^{(r)}} + gz\right) = 0, \tag{55}$$

$$-\mathrm{i}\omega v + fu - \frac{ik\beta}{K^2}v + il\left(\frac{p}{\rho^{(r)}} + gz\right) = 0. \tag{56}$$

Although some approximation is involved in the introduction of the β terms, they are brought into the equations through their interaction with the horizontal velocity, as they would be in the unapproximated equations, and they will therefore interact with the vertical grid staggering in the correct way.

The inclusion of the β-effect results in an equation set that is no longer isotropic in the horizontal wavevector (k, l). However, the effect of rotating the wavevector (keeping K constant) is simply to rescale the magnitude of the β-effect: it goes to zero when $k = 0$ and is a maximum when $l = 0$. It is sufficient, therefore, to restrict attention to the case $l = 0$, and only results for this case are presented in Section 5.

3. Analytical normal modes

When the reference state is isothermal, implying that the reference static stability $N^{(r)2} = g\theta_z^{(r)}/\theta^{(r)}$ and the reference sound speed squared $c^{(r)2} = RT^{(r)}/(1-\kappa)$ are both constant, the dispersion relation may be found analytically. This is most easily done by working in a height coordinate. Eliminating u, v, w, and θ from (46), (47), and (50), and the height-coordinate versions of (55) and (56), leaves an equation for p

$$\left(\frac{\partial}{\partial z} + A\right)\left(\frac{\partial}{\partial z} + B\right)p + Cp = 0, \tag{57}$$

where $A = N^{(r)2}/g$, $B = g/c^{(r)2}$, and

$$C = \left\{ \frac{1}{c^{(r)2}} + \left(K^2 + \frac{k\beta}{\omega} \right) \left[f^2 - \left(\omega + \frac{k\beta}{K^2} \right)^2 \right]^{-1} \right\} \left(\omega^2 - N^{(r)2} \right). \tag{58}$$

The boundary conditions expressed in terms of p are

$$\left(\frac{\partial}{\partial z} + B \right) p = 0 \tag{59}$$

at $z = 0$ and $z = D$.

It is straightforward to show (e.g. [32]) that (57) and (59) have two kinds of solution: external modes and internal modes. The external modes (also sometimes called Lamb modes) have an exponential vertical structure with w and θ zero everywhere, and satisfy the dispersion relation

$$\omega \left[f^2 - \left(\omega + k\beta/K^2 \right)^2 \right] + c^{(r)2} K^2 \left(\omega + k\beta/K^2 \right) = 0. \tag{60}$$

This is a cubic equation for ω, and the three roots correspond to two acoustic modes and a Rossby mode.

The internal modes have an exponentially weighted sinusoidal vertical structure with vertical wavenumber $m = n\pi/D$ where n is a positive integer. They satisfy the dispersion relation

$$\omega \left[c^{(r)2} \left(m^2 + \Gamma^2 \right) + N^{(r)2} - \omega^2 \right] \left[f^2 - \left(\omega + k\beta/K^2 \right)^2 \right] - c^{(r)2} K^2 \left(\omega + k\beta/K^2 \right) \left(\omega^2 - N^{(r)2} \right) = 0, \tag{61}$$

where $\Gamma = (B - A)/2$. This is a quintic equation for ω ; for every positive integer n there are five roots corresponding to two acoustic modes, two inertia-gravity modes, and a Rossby mode, and the corresponding mode structures have $n - 1$ zeros in the vertical profile of w.

The normal mode structures for other vertical coordinates may be found from those in height coordinates using the transformation rule for perturbation quantities ψ

$$\psi|_s = \psi|_z - s|_z \psi_s^{(r)} \tag{62}$$

(e.g. [18]). These are useful for checking correctness of the coding of the various configurations as well as for interpreting the results.

4. Computing normal modes of the discrete equations

As discussed already in Section 2, for each choice of vertical coordinate there are several possible choices for the pair of prognostic thermodynamic variables. For each of these choices there are various ways of staggering the variables. It is natural to store w at the boundaries in order to impose $w = 0$ there. Therefore, we will consider cases in which the other variables are staggered or not staggered relative to w. Moreover, it is clear from the governing equations (the Coriolis terms in particular) that inaccuracies due to vertical averaging will be introduced, with no advantage gained, if u and v are not stored at the same levels. Therefore, we will restrict attention to cases in which u and v are stored at the same levels. Thus, for each pair choice of prognostic variables there are 8 choices of vertical staggering, depending on whether (u, v) and the two thermodynamic variables are or are not staggered relative to w. Thus, for the height coordinate, isentropic coordinate, and terrain-following mass-based coordinate there are, respectively, $6 \times 8 = 48$, $6 \times 8 = 48$, and $9 \times 8 = 72$ configurations to consider. For the isentropic coordinate we consider both the p-form and the M-form of the equations. Many of these configurations could be rejected on general principles without detailed consideration. However, with suitable coding it is relatively straightforward to analyse all of them numerically, and some useful additional information can be gained by doing so.

For each of these cases, solutions proportional to $\exp i(kx + ly - \omega t)$ were assumed and the (advective-form) governing equations were discretized on a vertical grid with $N + 1$ w-levels, including top and bottom boundaries, and a grid spacing corresponding to constant Δz for the reference state. The results shown in Section 5 are for $N = 20$. Simple second-order accurate centred differences, over one or two grid intervals as appropriate, were used to approximate vertical derivatives, and a simple average of neighbouring values was used to transfer values from unstaggered to staggered levels or vice-versa when needed. (Using higher-order centred differencing is expected to have a minor impact on the results compared to changing the grid staggering; see [12].) The discretization results in a matrix eigenvalue problem of the form

$$\omega \mathbf{x} = \mathbf{A}\mathbf{x}, \tag{63}$$

where $\mathbf{x}$ is the state vector consisting of the values of all prognostic variables at all levels, and ω is the eigenvalue.

The length of the vector $\mathbf{x}$, i.e. the number of degrees of freedom available to the discretization, depends on the staggering of the variables. It is not necessary to store w at the boundaries: $N - 1$ values of w are stored. For the other variables, N values are stored if the variable is staggered relative to w, and $N + 1$ values are stored if the variable is not staggered. However, if z or θ is a predicted variable on w-levels then its boundary values are fixed at zero, thus suppressing two degrees of freedom. For the terrain-following mass-based coordinate, when z is predicted σ must be predicted too, giving an additional degree of freedom. The number of numerical eigenmodes should equal the number of degrees of freedom in the system. It is important to know whether each numerical eigenmode approximates a physical eigenmode or whether it is an unphysical or computational mode that could damage a numerical solution of the full equations. Identification of modes was aided by automatically counting zeros in the w and u fields.

The following parameter values were used: $D = 10{,}000$ m, $g = 9.80616$ m s^{-2}, $f = 1.031 \times 10^{-4}$ s^{-1}, $\beta = 1.619 \times 10^{-11}$ s^{-1} m^{-1} (corresponding to 45°N), $R = 287.05$ J kg^{-1} K^{-1}, $C_p = 1005.0$ J kg^{-1} K^{-1}, $T^{(r)} = 250$ K, and $k = 2\pi/10^6$ m^{-1}. Eq. (63) was solved using a standard numerical eigenvalue solver (NAG), and the resulting values of ω were compared with the analytical values.

5. Results

To summarize the results for the large number of configurations tested we divide them into five categories; configurations in the first four are shown in Table 1.

5.1. Category 1: Optimal

For each vertical coordinate, there is exactly one configuration that has no computational modes and has numerical dispersion properties distinctly better than all other configurations. These are therefore the optimal configurations for the representation of normal modes. The numerical dispersion relation for the optimal height-coordinate configuration is shown in Fig. 1. The dispersion relations for the optimal isentropic-coordinate and terrain-following-mass-based-coordinate configurations are virtually identical to this one. The frequencies of the numerical eigenmodes (crosses) agree well with those of the analytical eigenmodes predicted in Section 3 (diamonds). The figure shows only the westward propagating modes. There are two external modes (vertical mode zero): a high frequency acoustic mode and a low frequency Rossby mode. And there are three branches of internal modes (vertical mode greater than zero corresponding to n in Section 3): high frequency acoustic modes, medium frequency inertia-gravity modes, and low frequency Rossby modes. The eastward propagating modes (not shown) have only a single acoustic external mode and two branches of internal modes (acoustic and inertia-gravity). Their behaviour is extremely similar to that of the corresponding westward propagating modes.

Table 1
Summary of configurations in categories 1–4

Height coordinate	Isentropic coordinate	Terrain-following mass-based coordinate
Category 1		
$(w\theta, uvp)$	$(wz, uvM)^{\mathrm{M}}$ $(w, uv\sigma M)^{\mathrm{Ma}}$	$(w\theta, uvp)$
Category 2a (slow Rossby modes)		
$(w\theta, uv\rho)$	(wz, uvp)	$(w\theta z, uv)$
$(wT, uvp)^{\mathrm{b}}$	$(wp, uvM)^{\mathrm{Mb}}$	$(w\theta, uv\rho)$
Category 2b (fast Rossby modes)		
$(w\theta, uvT)$	$(wz, uv\sigma)^{\mathrm{P}}$	$(w\theta, uvT)^{\mathrm{u}}$
$(w\rho, uvp)^{\mathrm{b}}$		
Category 3		
$(w, uvp\rho)$ $(w, uvT\rho)$	$(w, uvpz)$	(wz, uvp) $(w, uvpT)$
$(w, uvp\theta)$ $(w, uv\theta\rho)$	$(w, uvp\sigma)$	(wz, uvT) $(w, uvT\rho)^{\mathrm{u}}$
$(w, uvpT)$ $(w, uv\theta T)$	$(w, uvpM)$	$(wz, uv\theta)$ $(w, uv\theta\rho)^{\mathrm{u}}$
	$(w, uvzM)$	$(w, uvp\rho)^{\mathrm{u}}$ $(w, uv\theta T)$
		$(w, uvp\theta)$
Category 4		
$(wuv\theta, p)$	$(wuvz, M)^{\mathrm{M}}$	$(wuv\theta, p)$

Superscript 'a' indicates that the configuration qualifies for category 1 only if one degree of freedom in σ is suppressed. Superscript 'b' indicates that the configuration qualifies for category 2 only if the boundary values of the thermodynamic variables are suppressed. Superscript 'P' or 'M' on isentropic-coordinate configurations indicates that only the p-form or M-form, respectively, qualifies for the stated category; no superscript indicates that both forms qualify. Superscript 'u' indicates that the configuration becomes unstable on a deeper $D = 50{,}000$ m domain.

One further configuration, the isentropic-coordinate $(w, uv\sigma M)^{\mathrm{M}}$ configuration, has numerical eigenmode frequencies virtually identical to those of the optimal configurations. It also has one zero-frequency computational mode, but, at least in the context of the linear calculations made here, it is a trivial computational mode and is easily suppressed. For this configuration, the profile of z must be diagnosed by imposing $z = 0$ at either the lower or upper boundary, and then integrating either upwards or downwards. The computational mode has all prognostic variables equal to zero except for the value of σ furthest from the boundary where $z = 0$ is applied; it corresponds to a non-zero value of z on the other boundary. However, that value of σ has no effect on any of the other prognostic variables; it is therefore a redundant degree of freedom, and dropping it would remove the computational mode. This configuration is indicated by superscript 'a' in the table.

5.2. Category 2: Near-optimal

For each vertical coordinate there are several configurations that have no computational modes and have good dispersion properties, though not as good as the optimal configuration. These near-optimal configurations fall into two groups: those that underestimate Rossby mode frequencies (category 2a—an example is shown in Fig. 2), and those that overestimate Rossby mode frequencies (category 2b—an example is shown in Fig. 3).

There are some configurations that could be included in category 2 except that they have two trivial computational modes associated with the use of a thermodynamic variable at the top and bottom boundaries; in fact those boundary thermodynamic variables play no role in the equations so they could be dropped,

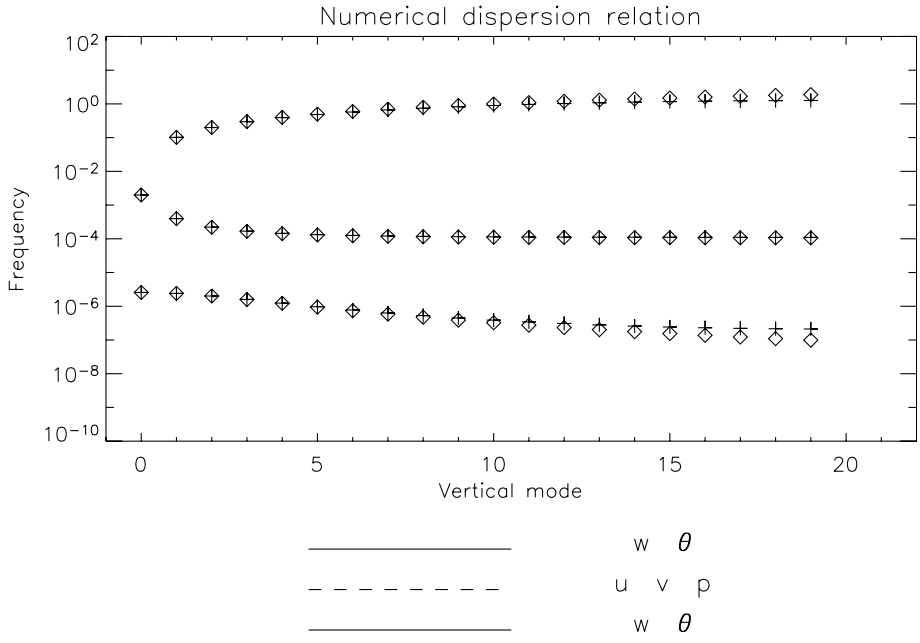

Fig. 1. Numerical dispersion relation (frequency in s^{-1}) for the optimal height-coordinate configuration ($w\theta, uvp$). The arrangement of variables on the grid is shown by the schematic underneath the main graph. Crosses indicate frequencies of numerical eigenmodes; diamonds indicate frequencies of analytical eigenmodes. Only westward propagating modes are shown; the behaviour of the eastward propagating acoustic and inertia-gravity modes is extremely similar to that of their westward-propagating counterparts.

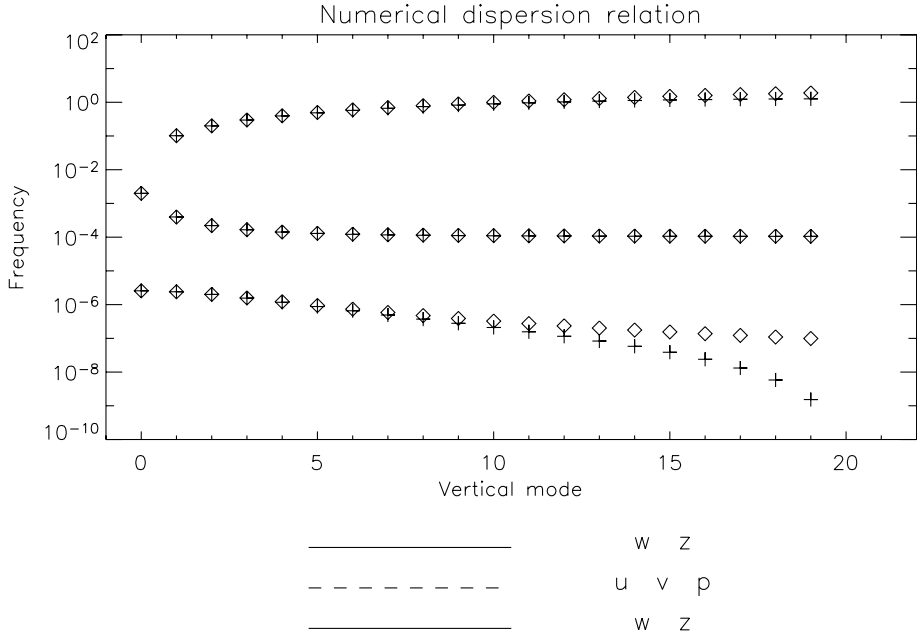

Fig. 2. Numerical dispersion relation for the category 2a isentropic-coordinate configuration (wz, uvp). Other details as in Fig. 1.

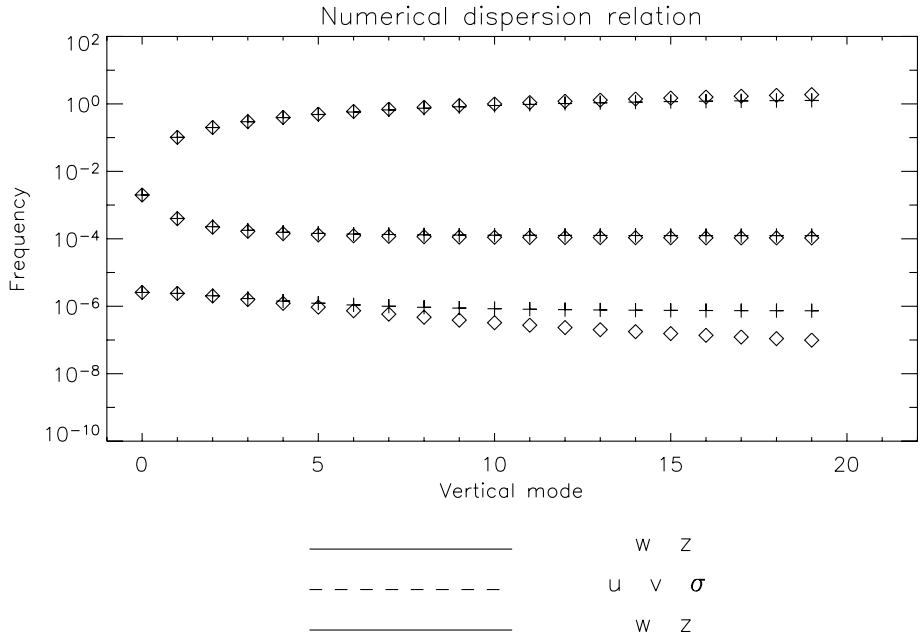

Fig. 3. Numerical dispersion relation for the category 2b isentropic-coordinate configuration ($wz,uv\sigma$). Other details as in Fig. 1.

eliminating two degrees of freedom and the computational modes. These configurations are indicated by superscript 'b' in the table.

5.3. Category 3: Single zero-frequency computational mode

Many configurations have good numerical dispersion properties (though not as good as the optimal configurations) except that they support a single computational mode of zero frequency. The computational modes consist of a pattern in one or both of the thermodynamic variables, often but not always involving a two-grid length oscillation, that is in hydrostatic balance and implies zero net horizontal pressure gradient plus geopotential gradient force. An example dispersion relation is shown in Fig. 4. All the others are almost identical, except for the isentropic coordinate configuration $(w,uvp\sigma)^{\mathrm{P}}$ which overestimates the frequencies of higher internal Rossby modes. Despite their computational mode, many of these configurations are of interest because they facilitate enforcement of desirable conservation properties (e.g. [30]).

5.4. Category 4: Inertial frequency decoupled modes

Some configurations can be shown theoretically to support a pair of modes with ω equal to the inertial frequency ($\pm f - k\beta/K^2$) that consist of two-grid-length oscillations in u and v decoupled from w and the thermodynamic variables. In terms of frequency and structure these modes are good numerical approximations to high internal inertia-gravity modes. The three category 4 configurations listed in the table support such modes and otherwise have quite good dispersion properties. However, they suffer a common problem in that just three modes, a high internal eastward inertia-gravity mode, a high internal westward inertia-gravity mode, and a high internal Rossby mode, are badly distorted. Note that the category 4 configurations are very similar to the optimal configurations except for the staggering of u and v.

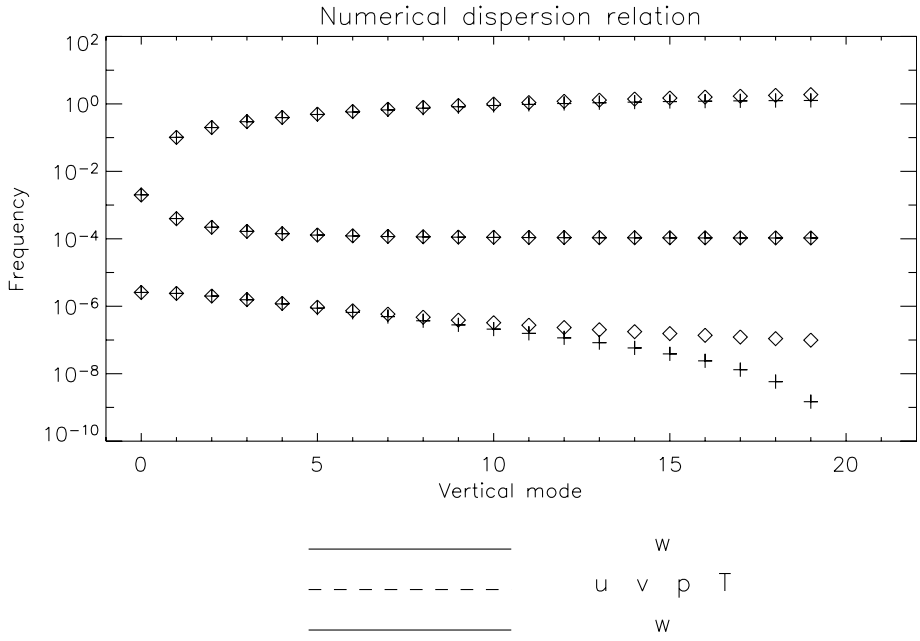

Fig. 4. Numerical dispersion relation for the category 3 terrain-following mass-based coordinate configuration ($w, uvpT$). Other details as in Fig. 1.

5.5. Category 5: The rest

The vast majority of the configurations considered are problematic in some way. The problems include having multiple computational modes, having modes that are so badly misrepresented in terms of frequency or structure that their physical counterparts cannot be identified, having part of the Rossby mode spectrum propagate eastward, and having unstable modes (i.e. modes whose eigenvalues ω have non-zero imaginary part).

6. Discussion

The optimal height-coordinate configuration is precisely that predicted in Section 1 on the basis of normal mode structures and consideration of the finite-difference equations. In fact the optimal isentropic-coordinate configuration can also be explained heuristically on the same basis: z perturbations on isentropes have essentially the same vertical structure as θ perturbations on height surfaces, and M perturbations on isentropes have essentially the same vertical structure as p perturbations on height surfaces, so that the isentropic-coordinate (wz, uvM) configuration is ideal for capturing the normal mode structures; and the finite-difference equations for the $(wz, uvM)^{\mathrm{M}}$ configuration minimize the occurrence of vertical averages and coarse vertical differences. It would be valuable to know whether this configuration, or a modification of it, remains optimal for a more general Lagrangian vertical coordinate. The optimal terrain-following mass-based coordinate configuration is very similar to the optimal height-coordinate configuration. Inspection of their finite difference schemes shows that they are very similar, with the main difference being the additional term involving z on u, v levels in the terrain-following mass-based coordinate. This z term is diagnosed by vertically integrating ρ on w levels, and this ρ is diagnosed from θ, which is already on w

levels, and p, which has been averaged to w levels. However, in the hydrostatic limit relevant to Rossby modes, the θ contribution to ρ dominates the p contribution, and thus the averaging of p to w levels is not detrimental. It is notable that there is no "perfect" configuration that completely avoids vertical averaging in the finite difference equations.

The isentropic-coordinate $(w, uv\sigma M)^{\mathrm{M}}$ configuration is particularly interesting: its numerical eigenmode frequencies are as accurate as those of the optimal configurations, and its mass variable σ is predicted on u, v levels, which should facilitate the enforcement of desirable conservation properties. However, it has a computational mode; this is a trivial one and easily suppressed in the linear normal mode calculations discussed here, but might not be in a fully non-linear model. Also, in a fully non-linear model, this configuration would require the solution of non-local, non-linear, simultaneous equations for z and p (the non-linear version of (27)); although not particularly difficult to solve, this would add to the complexity and cost of such a scheme. Incidentally, a configuration very similar to this one, $(-, uv\sigma)$, is found to have optimal dispersion properties for the hydrostatic primitive equations in an isentropic coordinate; in the hydrostatic case it has no computational mode. Finally, in an isentropic coordinate, potential vorticity might be considered an attractive choice of prognostic variable (e.g. [14,20]). In the linear normal mode analysis the potential vorticity perturbation Q is given by a linear combination of the wind and mass perturbations

$$\frac{Q}{Q^{(\mathrm{r})}} = \frac{\xi}{f} - \frac{\sigma}{\sigma^{(\mathrm{r})}}. \tag{64}$$

Therefore, the configuration $(w, Q\delta\sigma M)^{\mathrm{M}}$ should have the same dispersion properties as $(w, uv\sigma M)^{\mathrm{M}}$. This suggests that these two configurations deserve further investigation.

For the parameters given in Section 4, all the configurations in categories 1–3 have largest relative errors in frequency for the highest internal Rossby modes. For the resting basic state studied here these modes have very low frequency; for a realistic non-resting basic state their frequencies would be dominated by Doppler shifting and these errors would be much less noticable. These errors, and the differences between categories 1 and 2, might therefore be considered relatively unimportant.

The numerical dispersion relations were recomputed with a much shorter horizontal wavelength $k = 2\pi/10^4\ \mathrm{m}^{-1}$. All the categories listed in the table were found to be robust. However, for this value of k all the configurations in categories 1–3 capture the Rossby mode frequencies extremely accurately, and the largest relative errors are in the frequencies of the highest internal inertia-gravity modes. The numerical dispersion relations were also recomputed for a domain depth $D = 50{,}000$ m. Most of the categories listed in the table were found to be robust. However, four of the terrain-following mass-based coordinate configurations, indicated by superscript 'u' in the table, became unstable for the deeper domain. It is conceivable that a more careful choice of vertical averaging could allow these configurations to remain stable, but this has not been pursued here. Two other terrain-following mass-based coordinate configurations, $(w\theta, uvT)$ and $(w, uvpT)$, remained in the same categories for the deeper domain but some of their mode structures became so distorted that the modes could not be identified simply by counting zeros in their w and u profiles.

As should be expected theoretically, counting degrees of freedom is found to be an accurate guide to the existence of computational modes. First, when u and v are staggered relative to w, we can expect to be able to capture the structure of internal modes up to and including $n = N - 1 = 19$, plus the three external modes, making $5N - 2 = 98$ modes in total. It is found that configurations fall into categories 1 or 2 if and only if they have 98 degrees of freedom. Note that all configurations in categories 1–3 have u and v staggered relative to w. An important point is that different kinds of vertical averaging (e.g. the scheme of Taylor [30] rather than the simple averaging used here) cannot change the number of degrees of freedom and therefore cannot affect the number of computational modes.

When u and v are on w levels we might expect to be able to capture some of the internal modes up to $n = N = 20$, including any inertial-frequency decoupled modes (see Section 5). We found that the category 4 configurations come close to capturing $5N = 100$ modes with 100 degrees of freedom, but they distort

three of the highest internal modes. It is conceivable that a more careful choice of vertical averaging would enable these configurations to capture a full spectrum of modes accurately, but this has not been pursued here.

Among all the configurations tested, it is found that the Rossby mode part of the spectrum is well represented (i.e. no missing or badly distorted modes) only if the inertia-gravity mode part of the spectrum is also well represented, and, in turn, the inertia-gravity mode part of the spectrum is well represented only if the acoustic mode part of the spectrum is also well represented. Inspection of the governing equations shows that the terms that must be captured accurately for a good representation of internal acoustic modes are precisely those that must be captured accurately for a good representation of hydrostatic balance. This, in turn, is necessary (but not sufficient) for a good representation of inertia-gravity modes for horizontal wavelengths greater than about 10 km. Similarly, the terms that must be captured accurately for a good representation of inertia-gravity modes are precisely those that must be captured accurately for a good representation of geostrophic balance, which in turn is necessary (but not sufficient) for a good representation of Rossby modes.

For the height coordinate, numerical dispersion relations were also calculated using the flux form of the equations for ρ, T and p. With the exception of the $(w\rho, uvp)$ configuration, all the configurations in categories 1–4 showed no noticeable difference in their dispersion relation. The explanation for this insensitivity is as follows. For almost all configurations in categories 1–4 (this applies to all three vertical coordinates), the Rossby mode dispersion errors are dominated by the averaging of thermodynamic variables that appear in the momentum equations. In most cases the averaging damps the amplitude of the perturbation in one of the thermodynamic variables, reducing the net force on air parcels, leading to a reduction of mode frequencies. In some cases, like the height-coordinate $(w\theta, uvT)$ configuration, in which the net force is a residual of two opposing contributions, when one of those contributions is damped by averaging, the net force can increase, leading to an increase in mode frequencies. For the exceptional height-coordinate $(w\rho, uvp)$ configuration, the sign of the Rossby mode frequency error changes, and the configuration moves category from 2b to 2a, when the flux form of the ρ and p equations is used. This configuration actually involves no averaging of thermodynamic variables in the momentum equations, and its errors are dominated by averaging of the w and divergence terms in the ρ and p equations. This configuration is therefore sensitive to the treatment of those equations. In fact, experimentation with different combinations of advective and flux forms for the ρ and p equations shows that, for this configuration, the sign of the Rossby mode frequency errors is determined by the treatment of the ρ equation.

Many of the category 5 configurations were found to be unstable. This included many height-coordinate and terrain-following mass-based coordinate configurations of the form $(wuvT_1, T_2)$ and $(wuvzT_1, -)$ where T_1 and T_2 stand for any of θ, ρ, T or p. The unstable configurations include the terrain-following mass-based coordinate configuration $(wuvz\theta, -)$, which would otherwise be expected to behave quite well, perhaps belonging to category 4. Some understanding of the origin of the instability can be obtained by attempting to derive the discrete form of the wave energy equation in the height coordinate (e.g. [31]). For these configurations it is found that when the expression for wave energy involves a cross-term (i.e. a product of the two thermodynamic variables) then certain terms that cancel in the analytical derivation fail to cancel for the finite-difference scheme because they mix averaged and non-averaged contributions; thus the schemes are not energy conserving. The combination of p and θ does not involve a cross-term and these configurations are found to be stable. The combination of T and ρ does not involve a cross-term for the special case of the isothermal basic state studied here, and is found to be stable, but is predicted to be unstable for a more general basic state. All other combinations of thermodynamic variable involve a cross-term and are found to be unstable. It is conceivable that a more careful choice of vertical averaging could make these configurations energy conserving, but this has not been pursued here.

7. Conclusion

Numerical dispersion relations have been computed for a large number of vertical discretizations of the compressible Euler equations, involving different choices of vertical coordinate, thermodynamic prognostic variables, and vertical grid staggering. Optimal and near-optimal configurations are noted in the table. Some general understanding of the factors that affect the numerical dispersion properties has been obtained, which could provide useful guidance when considering other candidate configurations not addressed here (for example using other prognostic variables or vertical coordinates, including hybrid coordinates). In particular, the following points emerged. The heuristic arguments presented in the introduction concerning the normal mode structures, and the amount of averaging and coarse differencing in the finite difference scheme, are generally valid and useful guides to which configurations will be optimal. (However, the relative importance of the averaged terms for different flow regimes matters, not just the number of averaged terms.) The number of degrees of freedom in the discretization is an accurate guide to the existence of computational modes. There is only minor sensitivity to whether the equations for thermodynamic variables are discretized in advective form or flux form. Finally, an accurate representation of acoustic modes is a prerequisite for accurate representation of inertia-gravity modes, which, in turn, is a prerequisite for accurate representation of Rossby modes.

Acknowledgement

The authors thank Andrew Staniforth for stimulating discussions relating to this work and for valuable comments on a draft version of the paper.

References

[1] A. Arakawa, V.R. Lamb, Computational design of the basic dynamical processes of the UCLA general circulation model, Methods Comput. Phys. 17 (1977) 13–265.
[2] A. Arakawa, S. Moorthi, Baroclinic instability in vertically discrete systems, J. Atmos. Sci. 45 (1988) 1688–1707.
[3] L. Bonaventura, A semi-implicit semi-Lagrangian scheme using the height coordinate for a nonhydrostatic and fully elastic model of atmospheric flows, J. Comput. Phys. 158 (2000) 186–213.
[4] R. Bubnova, G. Hello, P. Bénard, J.-F. Geleyn, Integration of the fully elastic equations cast in the hydrostatic pressure terrain-following coordinate in the framework of the ARPEGE/Aladin NWP system, Mon. Wea. Rev. 123 (1995) 515–535.
[5] J.G. Charney, N.A. Phillips, Numerical integration of the quasi-geostrophic equations for barotropic and simple baroclinic flow, J. Meteorol. 10 (1953) 71–99.
[6] M.J.P. Cullen, T. Davies, M.H. Mawson, J.A. James, S.C. Coulter, A. Malcolm, An overview of numerical methods for the next generation UK NWP and climate model, in: C. Lin, R. Laprise, H. Ritchie (Eds.), Numerical Methods in Atmosphere and Ocean Modelling. The André J. Robert Memorial Volume, Canadian Meteorological and Oceanographic Society, 1997, pp. 425–444.
[7] R. Daley, The normal modes of the spherical non-hydrostatic equations with applications to the filtering of acoustic modes, Tellus 40A (1988) 96–106.
[8] T. Davies, A. Staniforth, N. Wood, J. Thuburn, Validity of anelastic and other equation sets as inferred from normal mode analysis, Q. J. Roy. Meteorol. Soc. 129 (2003) 2761–2775.
[9] J. Dudhia, A nonhydrostatic version of the Penn State-NCAR mesoscale model: validation tests and simulation of an Atlantic cyclone and cold front, Mon. Wea. Rev. 121 (1993) 1493–1513.
[10] D.R. Durran, Numerical Methods for Wave Equations in Geophysical Fluid Dynamics, Springer, Berlin, 1999.
[11] R. Ford, M.E. McIntyre, W.A. Norton, Balance and the slow quasimanifold: some explicit results, J. Atmos. Sci. 57 (2000) 1236–1254.
[12] M.S. Fox-Rabinovitz, Computational dispersion properties of vertically staggered grids for atmospheric models, Mon. Wea. Rev. 122 (1994) 377–392.
[13] M.S. Fox-Rabinovitz, Computational dispersion properties of 3D staggered grids for a nonhydrostatic anelastic system, Mon. Wea. Rev. 124 (1996) 498–510.

[14] A.R. Gregory, Numerical simulations of winter stratosphere dynamics, Ph.D. Thesis, University of Reading, 1999.
[15] B.J. Hoskins, A.J. Simmons, A multi-layer spectral model and the semi-implicit method, Q. J. Roy. Meteorol. Soc. 101 (1975) 637–655.
[16] Y.-J.G. Hsu, A. Arakawa, Numerical modelling of the atmosphere with an isentropic vertical coordinate, Mon. Wea. Rev. 118 (1990) 1933–1957.
[17] Z.I. Janjic, J.P. Gerrity Jr., S. Nickovic, An alternative approach to nonhydrostatic modeling, Mon. Wea. Rev. 129 (2001) 1164–1178.
[18] A. Kasahara, Various vertical coordinate systems used for numerical weather prediction, Mon. Wea. Rev. 102 (1974) 509–522.
[19] R. Laprise, The Euler equations of motion with hydrostatic pressure as an independent variable, Mon. Wea. Rev. 120 (1992) 197–207.
[20] Y. Li., J. Ruge, J.R. Bates, A. Brandt, A proposed adiabatic formulation of 3-dimensional global atmospheric models based on potential vorticity, Tellus 52 (2000) 129–139.
[21] S.-J. Lin, A "vertically Lagrangian" finite-volume dynamical core for global models, Mon. Wea. Rev. (2004) submitted.
[22] E.N. Lorenz, Energy and numerical weather prediction, Tellus 12 (1960) 364–373.
[23] J.-H. Qian, F.H.M. Semazzi, J.S. Scroggs, A global nonhydrostatic semi-Lagrangian atmospheric model with orography, Mon. Wea. Rev. 126 (1998) 747–771.
[24] D.A. Randall, Geostrophic adjustment and the finite-difference shallow-water equations, Mon. Wea. Rev. 122 (1994) 1373–1377.
[25] M. Satoh, Conservative scheme for the compressible nonhydrostatic models with the horizontally explicit and vertically implicit time integration scheme, Mon. Wea. Rev. 130 (2002) 1227–1245.
[26] S. Saujani, T.G. Shepherd, Comments on "Balance and the slow quasimanifold: some explicit results", J. Atmos. Sci. 59 (2002) 2874–2877.
[27] E.K. Schneider, An inconsistency in vertical discretization in some atmospheric models, Mon. Wea. Rev. 115 (1987) 2166–2169.
[28] J. Steppeler, H.-W. Bitzer, M. Minotte, L. Bonaventura, Nonhydrostatic atmospheric modelling using a z-coordinate representation, Mon. Wea. Rev. 130 (2002) 2143–2149.
[29] M. Tanguay, A. Robert, R. Laprise, A semi-implicit semi-Lagrangian fully compressible regional forecast model, Mon. Wea. Rev. 118 (1990) 1970–1980.
[30] K.E. Taylor, A vertical finite-difference scheme for hydrostatic and nonhydrostatic equations, Mon. Wea. Rev. 112 (1984) 1398–1402.
[31] J. Thuburn, N. Wood, A. Staniforth, Normal modes of deep atmospheres. I: spherical geometry, Q. J. Roy. Meteorol. Soc. 128 (2002) 1771–1792.
[32] J. Thuburn, N. Wood, A. Staniforth, Normal modes of deep atmospheres. II: f–F-plane geometry, Q. J. Roy. Meteorol. Soc. 128 (2002) 1793–1806.
[33] T. Tokioka, Some considerations on vertical differencing, J. Meteorol. Soc. Jpn. 56 (1978) 98–111.
[34] A.A. White, A view of the equations of meteorological dynamics and various approximations, in: J. Norbury, I. Roulstone (Eds.), Large-Scale Atmosphere-Ocean Dynamics I: Analytical Methods and Numerical Models, Cambridge University Press, Cambridge, 2002, pp. 1–100.
[35] R.T. Williams, On the formulation of finite-element prediction models, Mon. Wea. Rev. 109 (1981) 463–466.
[36] N. Wood, A. Staniforth, The deep-atmosphere Euler equations with a mass-based vertical coordinate, Q. J. Roy. Meteorol. Soc. 129 (2003) 1289–1300.
[37] K.-S. Yeh, J. Côté, S. Gravel, A. Méthot, A. Patoine, M. Roch, A. Staniforth, The CMC-MRB global environmental multiscale (GEM) model. Part III: nonhydrostatic formulation, Mon. Wea. Rev. 130 (2002) 339–356.